CrossMark

Effect of boreal spring precipitation anomaly pattern change in the late 1990s over tropical Pacific on the atmospheric teleconnection

Yuanyuan Guo[1] · Zhiping Wen[1,2,3] · Ruidan Chen[1,3] · Xiuzhen Li[1,3] · Xiu–Qun Yang[3,4]

Abstract

Observational evidence showed that the leading mode of precipitation variability over the tropical Pacific during boreal spring experienced a pronounced interdecadal change around the late 1990s, characterized by a precipitation pattern shift from an eastern Pacific (EP) type to a central Pacific (CP) type. The distinct impacts of such a precipitation pattern shift on the extratropical atmospheric teleconnection were examined. An apparent poleward teleconnection extending from the tropics to the North Atlantic region was observed after 1998, while, there was no significant teleconnection before 1998. To understand why only the CP–type precipitation mode is associated with a striking atmospheric teleconnection after 1998, diagnostic analyses with the Eliassen–Palm flux and Rossby wave source (RWS) based on the barotropic vorticity equation were performed. The results show that for the EP–type precipitation mode, no significant RWS anomalies appeared over the subtropical Pacific due to the opposite effect of the vortex stretching and absolute vorticity advection processes. For the CP–type precipitation mode, however, there are both significant vorticity forcing source over the subtropical CP and clear poleward–propagation of Rossby wave. The spatial distribution of the CP–type precipitation pattern tends to excite a conspicuous anomalous southerly and a well–organized negative vorticity center over the subtropical CP where both the mean absolute vorticity gradient and mean divergence flow are large, hence, the interaction between the heating–induced anomalous circulation and the basic state made the generation of Rossby waves conceivable and effective. Such corresponding teleconnection responses to the prescribed heating were also examined by using a Linear Baroclinic Model (LBM). It turned out that significant poleward teleconnection pattern is only caused by the CP–type precipitation mode, rather than by the EP–type precipitation mode. Further sensitive experiments demonstrated that the change in spring basic state before and after 1998 played a relatively minor role in exciting such a teleconnection pattern, when compared with the tropical precipitation anomaly pattern change.

Keywords Tropical Pacific precipitation · Teleconnection · Tropical–extratropical interaction · Interdecadal change

✉ Zhiping Wen
zpwen@Fudan.edu.cn

[1]   Center for Monsoon and Environment Research and School of Atmospheric Sciences, Sun Yat–sen University, Guangzhou, China

[2]   Institute of Atmospheric Sciences, Fudan University, Shanghai 200433, China

[3]   Jiangsu Collaborative Innovation Center for Climate Change, Nanjing, China

[4]   CMA–NJU Joint Laboratory for Climate Prediction Studies, School of Atmospheric Sciences, Nanjing University, Nanjing, China

1 Introduction

The variability of tropical precipitation has received much attention due to its pronounced fluctuation on different time–scales and its tremendous impacts on the atmospheric circulation both in the tropics and in the extratropics (Hoskins and Karoly 1981; McBride et al. 2003; Wu et al. 2012; Guo et al. 2015, 2017; Chu et al. 2017). Since tropical precipitation is primarily governed by the El Niño–Southern Oscillation (ENSO) in the interannual time scale, the interannual variation of tropical precipitation in the mature winter has been extensively investigated in previous studies (Ashok et al. 2007; Taschetto and England 2009; Weng et al. 2009; Chung and Li 2013; Guo et al. 2017). However, an

accumulation of evidence suggested that the precipitation during the boreal spring [March–May (MAM)] is also characterized by energetic variations on both the interannual and interdecadal time–scales, which are distinguish with those in other seasons (e.g. Cai and Cowan 2009; Taschetto and England 2009; Feng and Li 2011; Feng et al. 2011; Guo et al. 2016). On the interannual time scale, MAM was considered to be the time when the impacts of central Pacific (CP) and eastern Pacific (EP) El Niño are the most different from each other (Cai and Cowan 2009; Taschetto and England 2009). On the interdecadal timescale, Guo et al. (2016), which is referred as "GWW2016" thereafter for the sake of convenience, showed that the leading mode of the MAM precipitation anomaly has experienced a pronounced interdecadal change around 1998 over the tropical Pacific Ocean based on the empirical orthogonal function (EOF) analysis. In GWW2016 (see Figs. 2 and 3 in that work), the first mode of EOF analysis (EOF1) during the pre–1998 period (1980–1998) is characterized by a zonal dipole pattern with positive precipitation anomalies over the equatorial EP and negative ones over the equatorial western Pacific (WP). In contrast, the EOF1 during the post–1999 (1999–2013) shows a positive center over the equatorial CP and a negative center over the western North Pacific (WNP). That is, the main precipitation mode during the period of 1980–2013 experienced an interdecadal shift from the EP–type to the CP–type around 1998 in boreal spring. Further analyses found that such an interdecadal change of precipitation anomaly mode is tightly relevant to the interdecadal enhancement of zonal advection feedback over the equatorial CP, which favors the westward shift of the anomalous warm and wet center from EP to CP.

It was noted that the EP–type precipitation mode is closely associated with the occurrence of strong conventional El Niño events before the late 1990s, such as the 1982 and 1998 events. However, the 2015/16 El Niño, which is well–known as one of the strongest El Niño events during the past decades (Jacox et al. 2016; Chen et al. 2017; Lim et al. 2017; Paek et al. 2017), is suggested to be a mixed case of both the EP and CP type (Lim et al. 2017; Paek et al. 2017). Whether the interdecadal change in the precipitation mode in GWW2016 is still robust after taking into account the 2015/16 El Niño event remains unknown. To address this question, it is necessary to extend the studying period to the present (namely, 1980–2016).

It has been demonstrated that the diabatic heating variability associated with tropical anomalous precipitation has significant influence on the circulations both in the tropics and in the extratropics (Hoskins and Karoly 1981; McBride et al. 2003; Wu et al. 2012; Guo et al. 2015, 2017; Chu et al. 2017). Rossby wave propagation, which could be forced by the anomalous tropical diabatic heating, was considered as an important linkage between the extratropical circulation and tropical precipitation anomaly. Hence, extensive studies have been conducted to investigate the relationship between the tropical forcing and the extratropical teleconnection patterns (Wallace and Gutzler 1981; Yoo et al. 2012; Chu et al. 2013, 2017; Zheng et al. 2013; Park and An 2014; Guo et al. 2015, 2017; Jia et al. 2015). By considering the shift of tropical spring precipitation from the EP to CP type around 1998 (GWW2016), it is interesting to ask whether the extratropical teleconnection motivated by the different tropical precipitation anomaly pattern changes accordingly.

The objective of this study is to address the question whether the extratropical teleconnection pattern exhibits significant interdecadal variation accompanying with the interdecadal change in the tropical precipitation interannual variability. Better understanding of such interdacadal change of the interannual variability in the tropical and extratropical atmospheric circulation around the late 1990s can be useful for the improvement of the climate prediction on the interdecadal time scale. The rest of the paper is organized as follows. The dataset and methodology used in the present work are described in Sect. 2. The robustness of the interdecadal change in the leading mode of precipitation was discussed in Sect. 3. The possible impacts of the anomalous precipitation modes on the teleconnection patterns are examined in Sect. 4 and the numerical experiment results are shown in Sect. 5. Final section is devoted to summary and discussion.

2 Datasets and methodology

2.1 Data

The datasets used in this work consist of (1) monthly variables obtained from the European Centre for Medium–Range Weather Forecasts (ECMWF) Interim reanalysis data (ERA–Interim) with a horizontal resolution of $2.5° \times 2.5°$ (Dee et al. 2011); (2) monthly precipitation data from the Global Precipitation Climatology Project Version 2.2 (GPCPv2.2) with both the observations and satellite precipitation data onto $2.5° \times 2.5°$ global grids (Adler et al. 2003); (3) monthly mean Hadley Center sea surface temperature (HadISST) with horizontal resolution of $1° \times 1°$ (Rayner et al. 2003). The spring mean is the average of MAM. The climatology is taken as the average for the period of 1981–2010. Compared with GWW2016, all the datasets were updated to the spring of 2016 (covering from 1980 to 2016), in order to examine the robustness of the interdecadal change in the leading mode of precipitation around 1998 with the latest super El Niño considered.

2.2 Rossby wave source

Following the previous studies (Sardeshmukh and Hoskins 1988; Shimizu and de Cavalcanti 2011), the barotropic vorticity equation after decomposing the total wind into the divergent and rotational component can be written as:

$$\left(\frac{\partial}{\partial t} + V_\psi \cdot \nabla\right)\zeta = -\zeta D - V_\chi \cdot \nabla\zeta \tag{1}$$

where ζ is the absolute vorticity, V_χ is the divergence wind, V_ψ is the rotational wind and D is the horizontal divergence. The left hand of Eq. (1) can be considered as Rossby wave propagation terms. The right hand represents the Rossby wave forcing terms, namely, Rossby wave source (RWS), as described in Eq. (2):

$$S = -\zeta D - V_\chi \cdot \nabla\zeta \tag{2}$$

Here, S represents RWS term. The source of Rossby wave is associated with the divergent flow, divergence, absolute vorticity and its gradient. In Eq. (2), $-\zeta D$ is the vortex stretching term (or the divergence term) and the other is absolute vorticity advection by divergent flow. Equation (2) can be rewritten in the form of RWS anomaly:

$$S' = -\overline{\zeta}\nabla \cdot V_\chi' - \zeta'\nabla \cdot \overline{V_\chi} - V_\chi' \cdot \nabla\overline{\zeta} - \overline{V_\chi} \cdot \nabla\zeta' \tag{3}$$

$$S' = S1 + S2 + S3 + S4 \tag{4}$$

Here the prime represents the departure from the climatology and the overbar is the climatology. For convenience, these four terms are referred as *S1, S2, S3* and *S4* in Eq. (4). *S1* and *S2* are the vorticity source forced by the interaction between anomalous divergence and mean vorticity, and by the interaction between mean divergence and anomalous vorticity, respectively. *S3* denotes the mean absolute vorticity advection by anomalous divergence flow and *S4* represents the anomalous absolute vorticity advection by mean divergence flow. RWS is a helpful tool to examine the generation of Rossby waves excited by diabatic heating at both tropics and extratropics (Lu and Kim 2004; Kosaka and Nakamura 2006; Yu and Zwiers 2007; Johnson and Kosaka 2016). Thus, the forcing processes associated with heating–induced teleconnection patterns, namely the generation of Rossby waves, were examined by using RWS in the present study.

2.3 Plumb flux

Three–dimensional Eliassen–Palm flux, proposed by Plumb (1985), was widely used as a powerful diagnostic tool of the three–dimensional propagation of Rossby waves (e.g. Black and Dole 1993; Yu and Zwiers 2007). Following Plumb

(1985), the horizontal component of the Plumb flux in the form of geostrophic wind can be written as:

$$F_H = p\cos\phi \times \begin{pmatrix} v'^2 - \frac{1}{2\Omega R\sin 2\phi}\frac{\partial(v'\Phi')}{\partial\lambda} \\ -u'v' + \frac{1}{2\Omega R\sin 2\phi}\frac{\partial(u'\Phi')}{\partial\lambda} \end{pmatrix} \tag{5}$$

Here, u, v are the horizontal geostrophic wind, Φ is the geopotential, Ω is the Earth's rotation rate, R is the Earth's radius, $p = pressure/1000\ mb$ and (φ, λ) are latitude and longitude, respectively. The perturbations deviating from the time mean are denoted by primes. With the application of this Plumb flux, the features of Rossby wave propagation incited by different diabatic heating patterns could be identified.

2.4 Linear baroclinic model (LBM)

LBM is a simple dry model, based on a linearized atmospheric general circulation model (AGCM) developed at the Center for Climate System Research (CCSR), University of Tokyo, and the National Institute for Environmental Studies (NIES), Japan (Watanabe and Kimoto 2000). It was widely used to examine the atmospheric response to the idealized diabatic heating (e.g. Peng and Whitaker 1999; Watanabe and Kimoto 2000; Lu and Lin 2009; Guo et al. 2015; Wang et al. 2016). The version with a horizontal resolution of T42 and 20 vertical levels using a sigma coordinate system is used in this study. The specific heating patterns were imposed into this model (using a time integration method and running up to 30 days) and the last 10–day average, referring as the steady atmospheric response to such prescribed diabatic heating, was analyzed.

3 The interdecadal change in anomalous precipitation pattern with the 2015/16 El Niño considered

Based on the leading mode of precipitation anomalies over the tropical Pacific during 1980–2013, the corresponding principal component (PC) exhibits a sudden flatness after 1998 (GWW2016). GWW2016 has demonstrated that the CP–type precipitation pattern becomes the dominant mode after 1998 while the EP–type one blurred to some degree. Hence, the robustness of such an interdecadal change of the interannual variability in precipitation mode was investigated in the present section by extending the study period to 2016 spring.

The precipitation and sea surface temperature (SST) anomaly patterns in the decaying spring of three strong El Niño cases (1983/1998/2016) were shown in Fig. 1. The SST
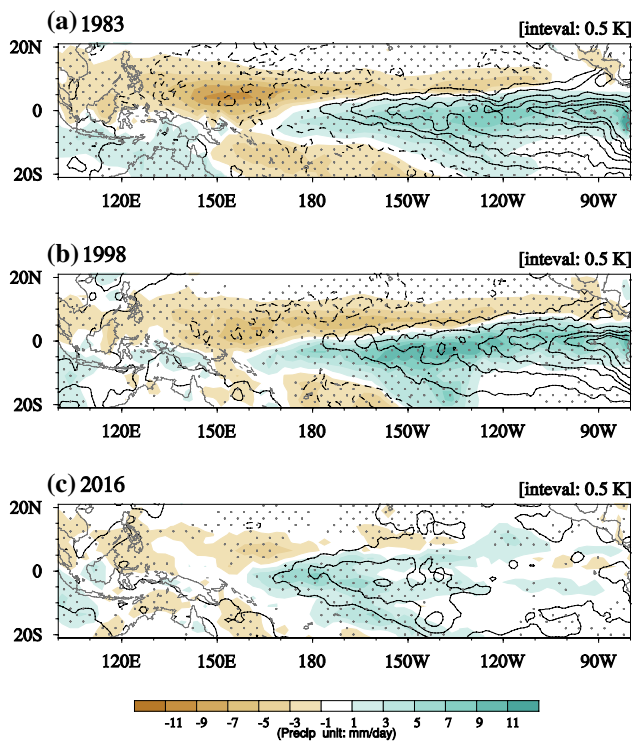
Fig. 1 Spatial pattern of the anomalies of precipitation (shading, unit: mm day^{-1}) and sea surface temperature (SST) (contour, unit: K) in the spring of **a** 1983, **b** 1998 and **c** 2016. The interval of SST anomaly contour is 0.5 K. The stippling indicates significance at the 99% confidence level

and the associated precipitation anomalies in 1983 and 1998 exhibit a zonal dipole pattern with warm/wet condition over the central–eastern Pacific and cold/dry over the western Pacific (Fig. 1a, b), which resembles the typical SST and precipitation distribution of EP–type precipitation mode. In 2016, the center of both SST and precipitation anomalies shifted to the central Pacific with weaker SST anomalies (Fig. 1c). The maximum of the SST anomaly center is up to 1K in 2016, compared to the other two case (up to 3K in 1983 and 1998). Precipitation anomaly pattern in 2016 showed similar features as the CP–type mode to some extent (Figs. 1b, 3a in GWW2016), implying that the CP–type precipitation mode may be still dominant after 1998.

To verify it, an EOF analysis was performed based on the MAM precipitation anomaly from 1980 to 2016 (Fig. 2). After extending the study period to 2016, the principal component of the first EOF mode (PC1, red line in Fig. 2c) still exhibits a sudden flatness after 1998. The principal component of the second EOF mode (PC2) shows pronounced interannual variability during the whole period, possibly becoming a leading mode after 1998. The EOF analysis during 1980 to 2016 is consistent with our previous work (see Fig. 1 in GWW2016). The result is indicative of a significant change in the interannual precipitation variability

around 1998. The EOF method was also applied during the pre–1998 (1980–1998) and post–1999 (1999–2016) period respectively with the associated PC1s presented in Fig. 2c. Noted that the pre–1998 PC1 is greatly consistent with the PC1 for 1980–2016 period and the post–1999 PC1 is in line with the PC2 for the whole period, verifying that the leading mode shifts from an EP–type pattern to a CP–type pattern around 1998. An interdecadal westward shift of the tropical precipitation leading mode around 1998/99 in boreal winter has also been noted in Jo et al. (2015). There may be a need of further examination to figure out the seasonal evolution of tropical precipitation mode from winter to spring on the interdecadal time scale. However, it is out of the scope in the present work. Overall, the observational results in the present work reveal that such an interdecadal change in the leading mode of tropical precipitation is robust even though the latest super El Niño occurred.

Accompanied by the interdecadal shift of the tropical precipitation interannual variation around 1998/99, the associated atmospheric circulation and SST anomaly patterns have been accordingly changed (figure not shown). For instance, the leading mode of tropical Pacific SST anomaly in spring shifted from an EP to a CP type after 1998 (see Fig. 4 in GWW2016). Simultaneously, the regressed vertical velocity anomalies at 500 hPa onto the post–1999 PC1 exhibit a zonal pattern with anomalous ascending over the equatorial CP and anomalous sinking over the WNP. In contrast, the anomalous Walker circulation during the pre–1998 period locates more eastward than that during the post–1999 period. These changes in the associated atmospheric circulation and oceanic condition around 1998/99 were statistically significant and distinguishable, giving us confidence to further analyzing the different teleconnection patterns related to distinct precipitation modes.

4 A significant teleconnection associated with the CP–type precipitation pattern after 1998

4.1 Observational evidence

By considering the remarkable change in the leading mode of spring precipitation around 1998, it is worthy to investigate whether the atmospheric circulation modulated by the distinguishable precipitation modes differs. To achieve this, the regression maps of precipitation and vertically integrated diabatic heating anomalies onto the pre–1998 and post–1999 PC1s were shown in Fig. 3. During the pre–1998 period, the dominant precipitation pattern is identified as an EP type, with negative precipitation anomalies over the WP and northern CP near the equator, and positive precipitation anomalies over the equatorial central–eastern Pacific when

Fig. 2 Spatial distribution of **a** the first EOF mode, **b** the second EOF mode and **c** the corresponding principle components (PCs, red and blue lines) of the precipitation anomalies over the tropical Pacific in spring for the period of 1980–2016. The black and green dash lines denote the PCs of the first EOF precipitation mode for the period of 1980–1998 and 1999–2016, respectively
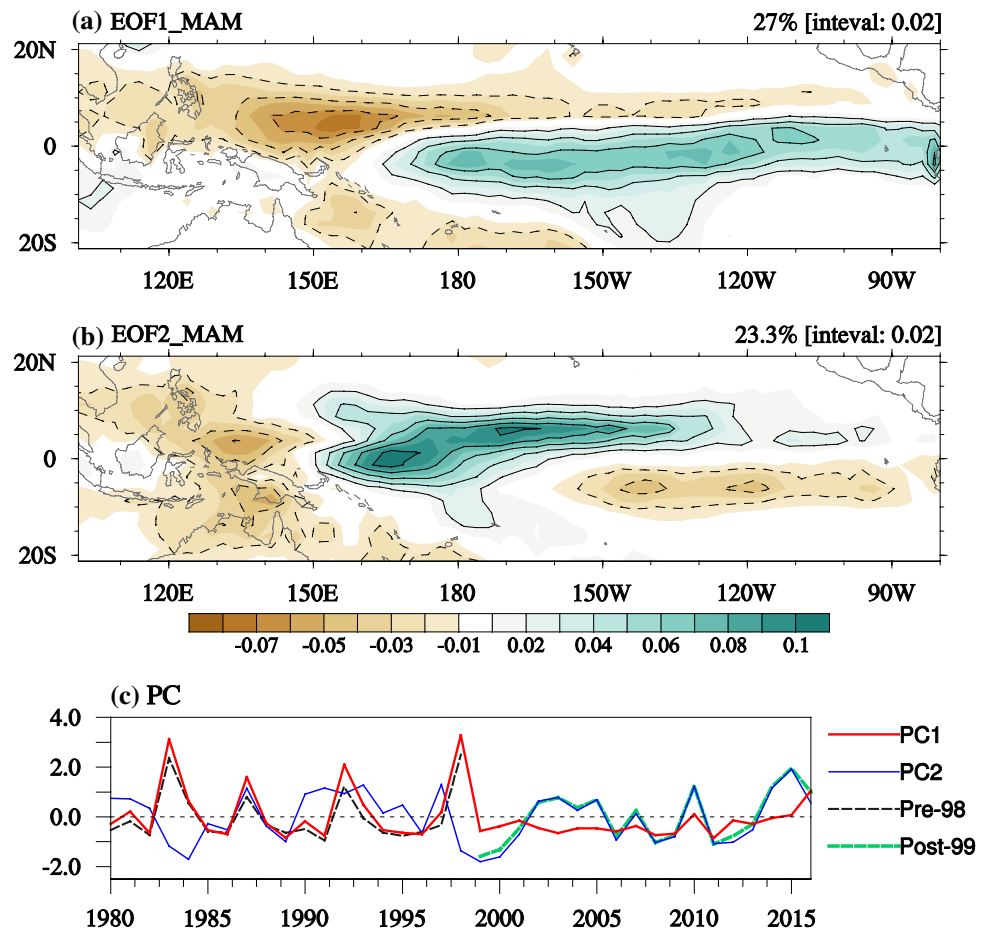
the pre–1998 PC1 is positive. In contrast, a triple pattern (dry condition over the WNP and the equatorial southeastern Pacific; wet condition over the equatorial and subtropical CP) appears over the tropical Pacific during the post–1999 period, which is identified as a CP type. The corresponding diabatic heating anomaly matches precipitation very well. The maximum of the vertical integrated diabatic heating is about 11.9 W m^{-2} for the EP warming region and -11.0 W m^{-2} for the WP cooling region during the pre-1998 period (Fig. 3a). During the post-1999 period, the regressed heating forcing is 11.4 W m^{-2} over the CP and -7.7 W m^{-2} over the WNP (Fig. 3b). As a response to the different heating patterns, the distinguishable atmospheric teleconnection circulations were proposed in this study.
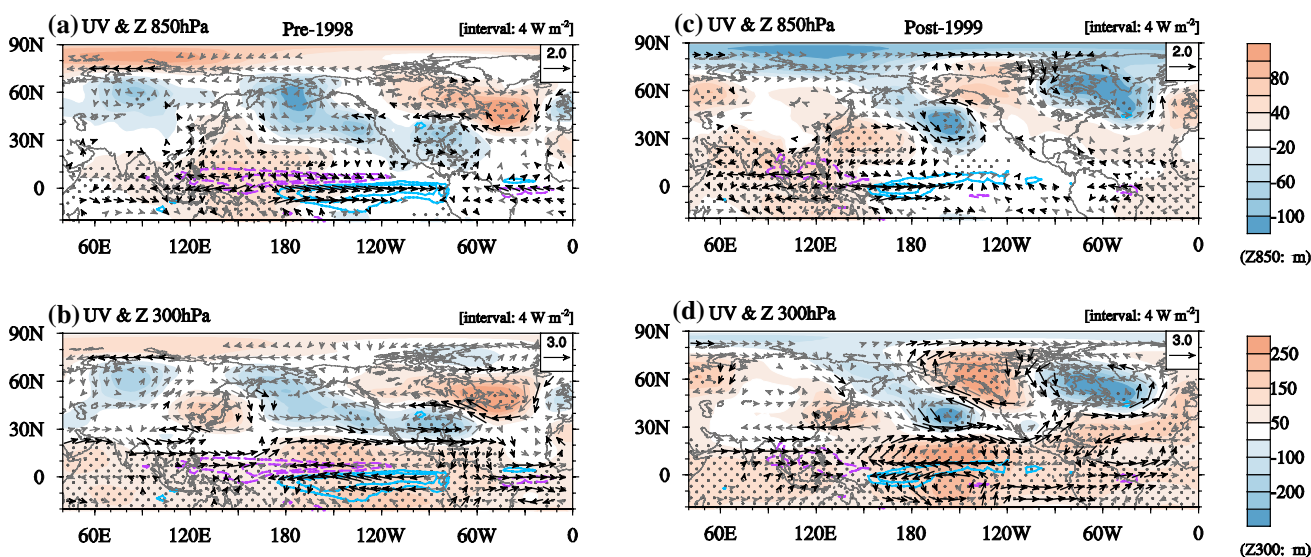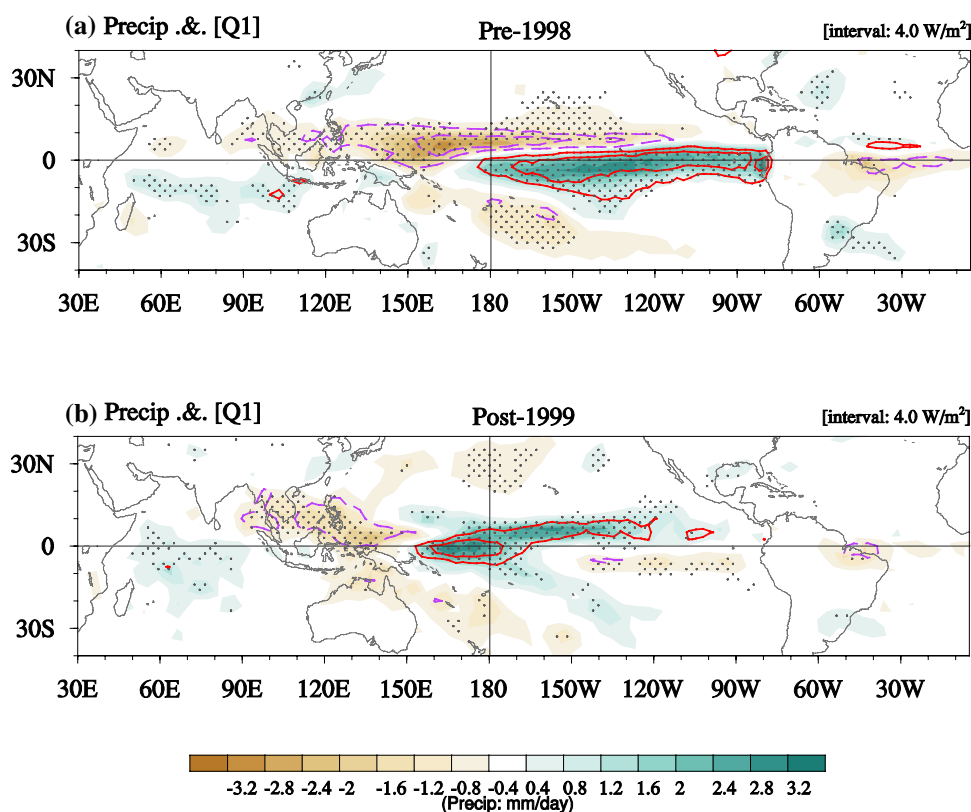
The regressed geopotential height and horizontal wind at lower and upper level were presented in Fig. 4. For the EP–type precipitation mode, a pair of significant anticyclonic centers straddles over the equatorial central–eastern Pacific at the upper level (Fig. 4b). Anomalous cyclonic and anticyclonic circulation appear over the eastern United States and North Atlantic Ocean with a barotropic structure, while the anticylonic circulation over the tropical EP is somewhat with a baroclinic structure. Besides, an anomalous cyclonic center

located over the North Pacific, however, is insignificant and feeble (Fig. 4a, b). In term of the CP–type pattern after 1998, alternating positive and negative centers extend from the tropical Pacific to North Atlantic Ocean at the lower level (Fig. 4c), following the great circle route (Hoskins and Karoly 1981). A more apparent teleconnection pattern was observed in the upper level (300 hPa), with anomalous anticyclonic circulation over the central–eastern Pacific, cyclonic center over the North Pacific, anticyclonic center over western Canada, cyclonic circulation over the North Atlantic Ocean and relatively feeble anticyclonic circulation over the tropical Atlantic (Fig. 4d). That is, the CP–type precipitation mode during the post–1999 period was closely associated with a pronounced teleconnection pattern propagating from the tropics to the Arctic Pole, while the teleconnection pattern over the North Pacific during the pre–1998 period is quite weak.

4.2 Possible mechanism of the distinct teleconnection associated with EP and CP type precipitation patterns

For the underlying processes in the stimulation of extratropical atmospheric circulation by the tropical diabatic heating,

Fig. 3 Regression maps of the precipitation anomalies (shading; unit: mm day^{-1}) and diabatic heating anomalies integrated from 1000 hPa to 100 hPa (contour; unit: W m^{-2}) onto the **a** pre–1998 PC1 and **b** post–1999 PC1. The contour interval for diabatic heating is 4.0 W m^{-2}. The stippling indicates significance at the 95% confidence level

Fig. 4 Regression maps of the geopotential height (shading; unit: m), horizontal winds (gray vector; unit: m s^{-1}) and vertically integrated diabatic heating anomalies (contour; unit: W m^{-2}) onto the **a, b** pre–1998 PC1 and **c, d** post–1999 PC1 at (upper panel) 850 hPa and (bottom panel) 300 hPa. The stippling and black vectors indicate significance at the 95% confidence level

many previous studies emphasized the Rossby wave propagation (e.g. Hoskins and Ambrizzi 1993; Webster and Chang 1998; Yoo et al. 2012; Guo et al. 2015, 2017). The forcing and propagating processes of heating–induced Rossby waves were carefully examined by the regressions of the

RWS and Plum flux onto the pre–1998 and post–1999 PC1s, respectively (Fig. 5). During the pre–1998 period, the RWS anomalies are significant over the tropical CP and EP and extremely weak over the subtropical Pacific. Besides, no evident poleward–propagating Plumb flux anomalies appear

in the extratropic (Fig. 5a). Hence, it is suggested that the feeble teleconnection pattern associated with the EP precipitation mode may be ascribed to the weak generation and propagation of Rossby waves. In contrast, significant negative RWS anomalies appear over the northern CP (between 10°N–20°N and 155°E–150°W) during the post–1999 period, accompanied by a striking northward/northeastward propagation of Plumb flux (Fig. 5b). The CP–type precipitation pattern might favor the generation of vorticity source over the northern CP and thus the propagation of Rossby waves. Since RWS is composed of the vortex stretching term and vorticity advection term, the relative contributions of these two terms before and after 1998 were examined (Fig. 6). During the pre–1998 period, vortex stretching term is opposite to the vorticity advection term over the CP to the north of 10°N (Fig. 6a, b). Their combined effects could not effectively generate the significant vorticity source before 1998. On the contrary, both vortex stretching and vorticity advection term feature significant negative anomalies over the northern CP (Fig. 6c, d). The contribution rate of vortex stretching term to the total RWS (within the box in Fig. 6c) after 1998 is approximately 67%, much higher than that of the vorticity advection term (33%, within the box in Fig. 6d). In sum, the weak (significant) teleconnection pattern might

result from the adverse (reinforced) effect of vortex stretching process and absolute vorticity advection by divergence flow during the pre–1998 (post–1999) period.

To further explain why only CP–type precipitation mode after 1998 is associated with remarkable generation and propagation of Rossby waves, the four terms (S1–S4) in Eq. (4), that is, the interaction processes between the mean state ($\overline{V}_\chi$ and $\overline{\zeta}$) and perturbations (V'_χ and ζ'), were examined. The regression maps of S1–S4 during the pre–1998 period were shown as Fig. 7. Note that the variables with primes indicate the regressions onto the pre–1998 and post–1999 PC1s, which could be considered as the anomalous circulation induced by the different precipitation modes. For the S1 term ($-\overline{\zeta}\nabla \cdot V'_\chi$), the interaction between the mean absolute vorticity and the heating–related divergence, is extremely weak in tropics due to the small climatological absolute vorticity. The mean absolute vorticity increases along the latitude and its gradient is large over the East Asian westerly jet region and subtropical central–eastern Pacific between 10°N and 30°N, where the isolines of absolute vorticity are dense (contours in Fig. 7a). The anomalous divergence flow associated with the EP–type precipitation mode shows convergence over the tropical WP and CP and divergence

Fig. 5 Regression maps of the 300–hPa Rossby wave source (RWS) (shading; unit: s^{-2}), horizontal Plumb flux (vector; unit: $m^2 \ s^{-2}$) and vertically integrated diabatic heating anomalies (contour; unit: $W \ m^{-2}$) onto the **a** pre–1998 PC1 and **b** post–1999 PC1. The contour interval for diabatic heating is 4.0 $W \ m^{-2}$. The stippling indicates significance at the 95% confidence level
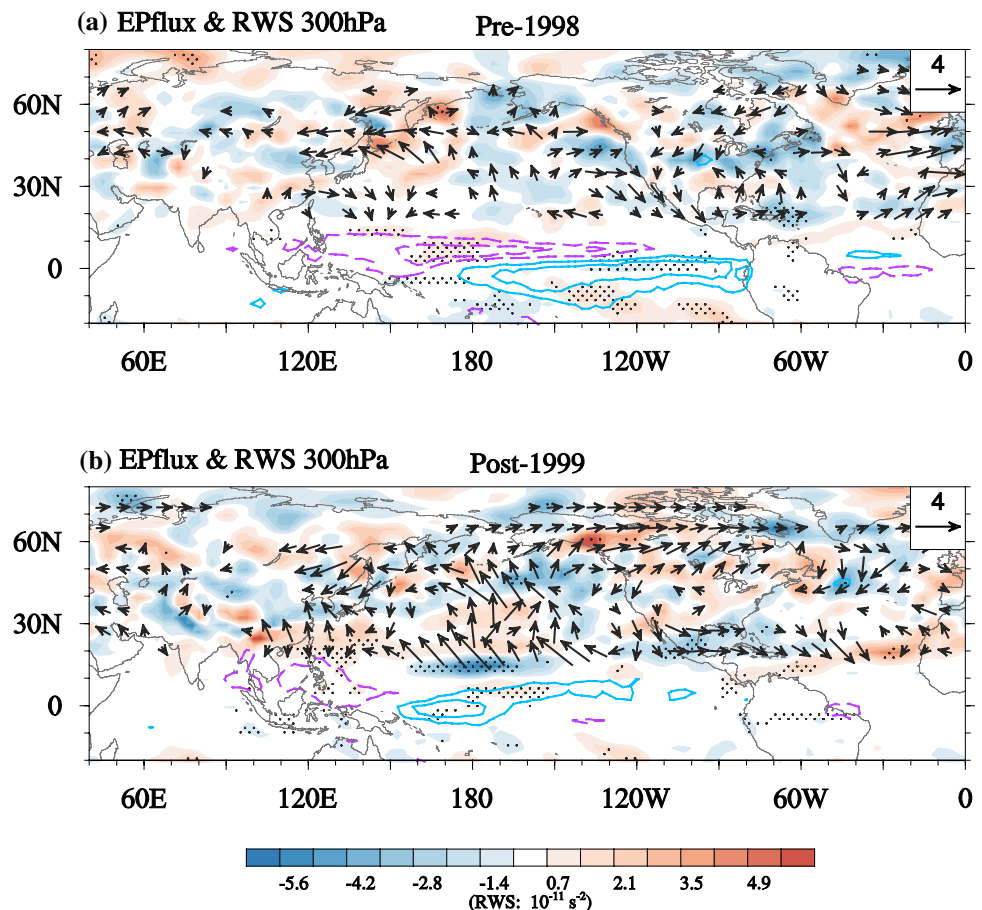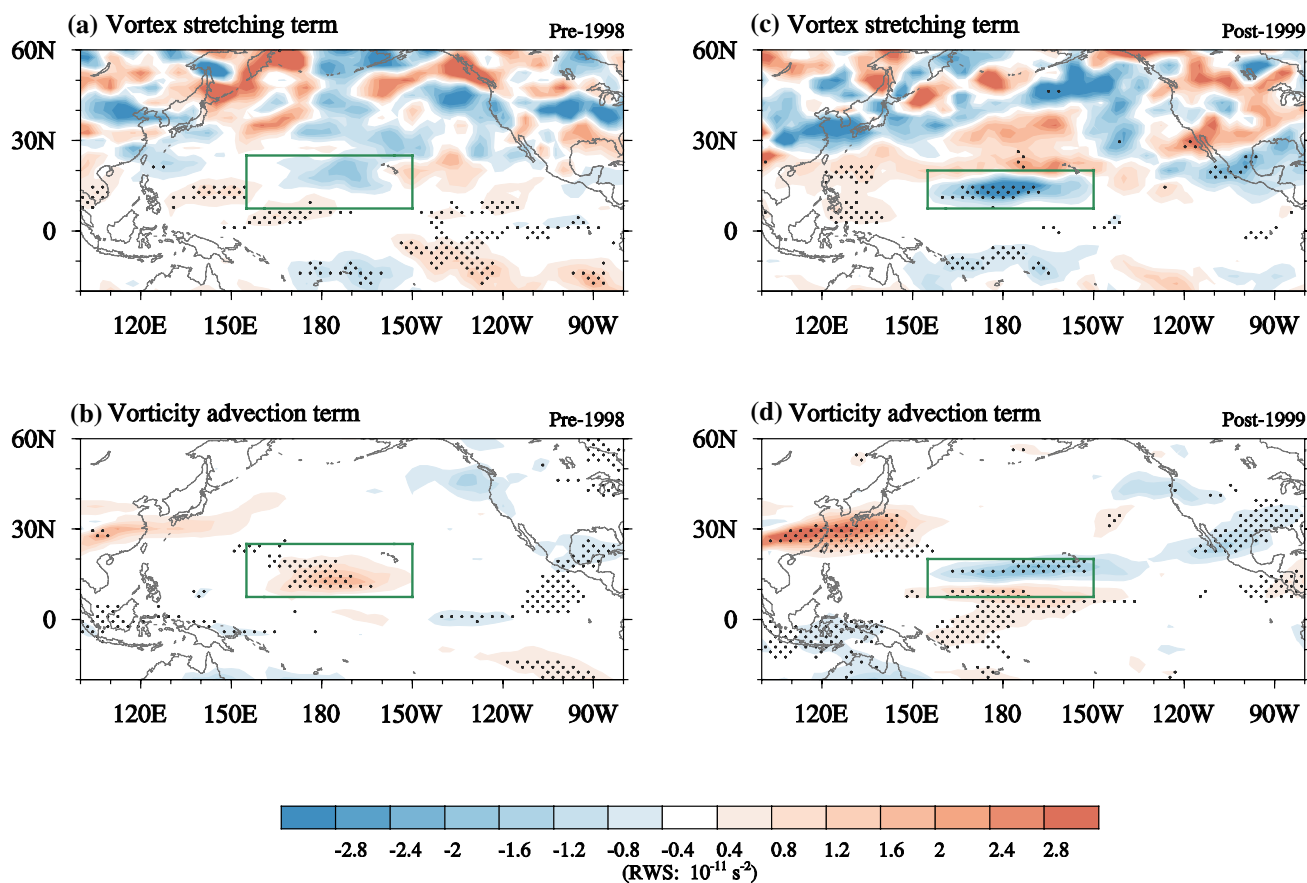
Fig. 6 Regression maps of the (upper panel) vortex stretching and (bottom panel) absolute vorticity advection terms shown in Eq. (2) onto the **a, b** pre–1998 PC1 and **c, d** post–1999 PC1 at 300 hPa. The stippling indicates significance at the 95% confidence level.

The boxes in (**a**) and (**b**) denote the focused area (7.5°N–25°N; 155°E–150°W). In (**c**) and (**d**), the boxes represent the area between 7.5°N–20°N and 155°E–150°W

over the tropical EP (vectors in Fig. 7a). To the north of 10°N, negative S1 anomalies appear over the subtropical CP, where the divergence anomalies are significant and mean absolute vorticity is large. For the S2 $(-\zeta' \nabla \cdot \overline{V_\chi})$, the interactive process between anomalous absolute vorticity and mean divergence, is negative over the northern CP. It is jointly contributed by the coupling of climatological southerly wind and the anomalous negative vorticity (contours in Fig. 7b) excited by the EP precipitation pattern. S3 term $(-V'_\chi \cdot \nabla\overline{\zeta})$, that is, the mean absolute vorticity advection by anomalous divergence flow, is featured by positive anomalies over the northern CP region (within the target area in Fig. 7c). The anomalous northerly associated with the EP–type precipitation mode, together with large absolute vorticity gradient, gives rise to the significant S3 anomalies. Because of the deformed and weak vorticity anomaly between 170°E and 120°W induced by the specific EP precipitation mode, S4 term is trivial over the northern CP and EP (Fig. 7d). Overall, the opposite effect of S1 and S3 (consistent with Fig. 6a, b) leads to

the insignificant RWS anomalies during the pre–1998 period. The S3 term $(-V'_\chi \cdot \nabla\overline{\zeta} > 0)$ offset S1 $(-\overline{\zeta}\nabla \cdot V'_\chi < 0)$ possibly due to the heating–induced northerly wind $(V'_\chi < 0)$ over the studying area and the divergence to its north $(\nabla \cdot V'_\chi > 0)$. In short, the divergence flow excited by tropical EP precipitation anomalies plays a vital role in the feeble teleconnection pattern during the pre–1998 period.

The behaviors of S1–S4 vary greatly during the post–1999 period (Fig. 8). The CP–type precipitation pattern is associated with a well–organized convergence flow over the WNP and divergence flow over the CP (vectors in Fig. 8a, c) and a zonal–elongated strong negative vorticity center over the northern CP (contours in Fig. 8b, d). Hence, such strong divergence flow induced by tropical diabatic heating, together with the mean absolute vorticity distribution and its gradient, causes the significant negative S1 and S3 anomalies over the northern CP (Fig. 8a, c). In addition, the interaction between the heating–excited negative vorticity center and climatological convergence

Pre-1998
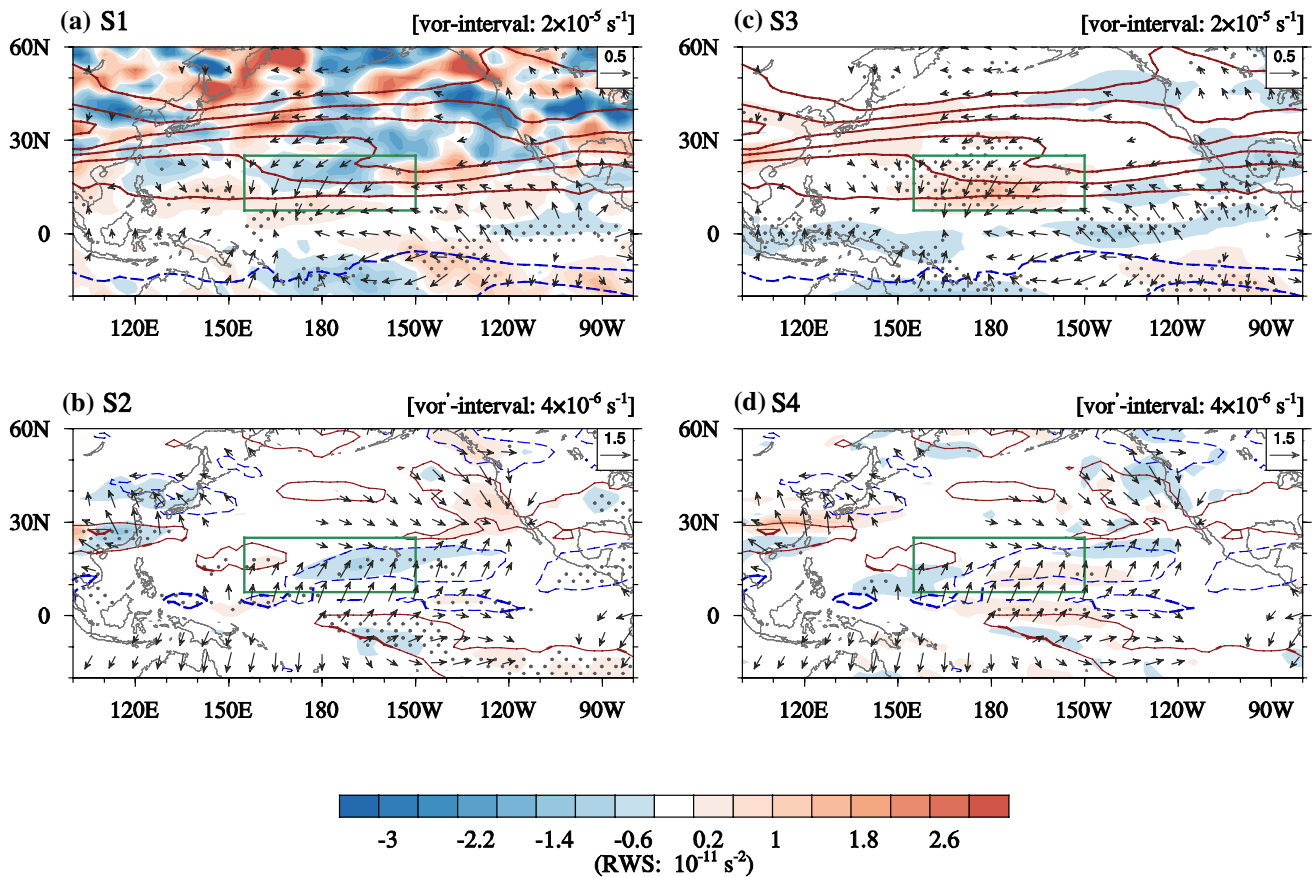
Fig. 7 Regression maps of the S1–S4 anomalies (shading; unit: s^{-2}) onto the pre–1998 PC1. In (**a**) and (**c**), the contour denotes the mean absolute vorticity for 1980–1998 and the vector is the regressed divergence wind onto the pre–1998 PC1 at 300 hPa. In (**b**) and (**d**), the contour denotes the regressed absolute vorticity onto the pre–1998 PC1 and the vector is the mean divergence wind for 1980–1998 at 300 hPa. The stippling indicates significance at the 95% confidence level. The boxes denote the area (7.5°N–25°N; 155°E–150°W)

favors the significant negative anomalies of S2 (Fig. 8b). S4 term ($-\overline{V}_\chi \cdot \nabla\zeta'$) is partly determined by the gradient of anomalous absolute vorticity. Hence, weak negative S4 anomalies are observed to the north of this negative absolute vorticity center and strong positive S4 anomalies to its south (Fig. 8d). All of the four physical processes contribute to the total RWS anomalies over our interested area (Fig. 5b). Over the target area, the area-averaged S2 term approximately offsets the area-averaged S4 term. The contribution rates of S1 and S3 to the total value are 39.5 and 60.5%, respectively, suggesting a relative dominant role of S3. Consequently, both the anomalous divergence southerly flow and negative absolute vorticity exert great impacts on the generation of Rossby wave and the observational teleconnection pattern from the tropics to mid–high latitudes after 1998.

In sum, the observational evidence shows that the EP–type precipitation mode is associated with a shapeless vorticity anomaly center and weak divergence flow to the north of the precipitation center, leading to a feeble tele-connection pattern at the mid–high latitudes. The CP–type precipitation pattern, which could induce a well–organized vorticity anomaly center and significant divergence southerly, possibly results in the effective generation of Rossby wave.

5 Numerical results

It has been demonstrated that the divergence flow and vorticity anomaly induced by distinguishable precipitation modes might primarily determine the existence of significant teleconnection patterns. To further verify our hypothesis, several experiments based on LBM were carried out (Table 1).

Post-1999
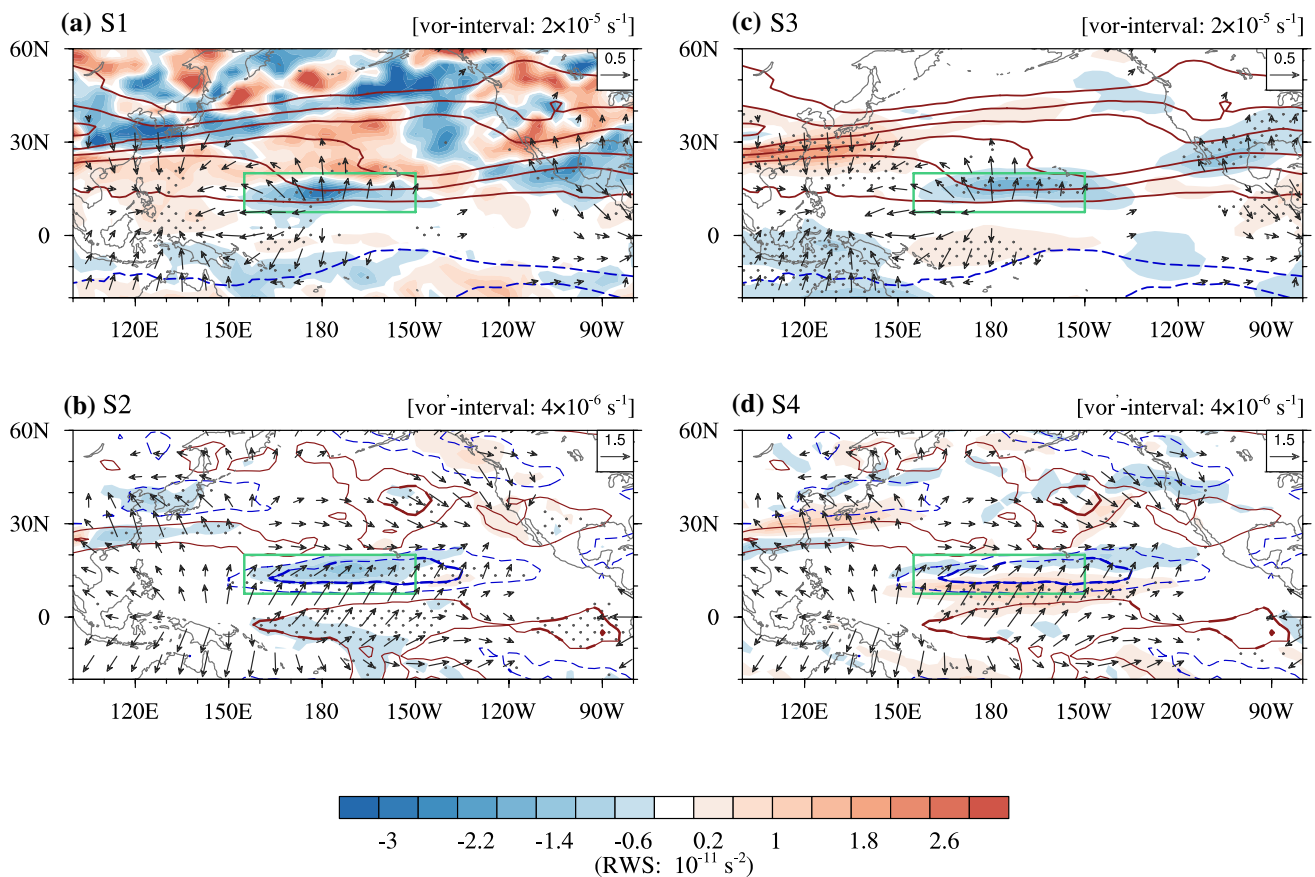
Fig. 8 Same as Fig. 7, but onto the post–1999 PC1. The mean absolute vorticity and divergence wind are averaged during 1999–2016. The boxes denote the area (7.5°N–20°N; 155°E–150°W)

Table 1 Four groups of the numerical experiments, including the details of heat forcing and basic state imposed into LBM

| Experiment	Forcing		Basic state
Exp. 1	EP–type	WP − only	1980–1998
		EP − only	*(pre–1998)*
		WP+EP	
Exp. 2	CP–type	WNP − only	1999–2016
		CP − only	*(post–1999)*
		WNP+CP	
Exp. 3	EP–type	WP − only	1999–2016
		EP − only	*(post–1999)*
		WP+EP	
Exp. 4	CP–type	WNP − only	1980–1998
		CP − only	*(pre–1998)*
		WNP+CP	

5.1 LBM experiments

The spatial distributions of the ideal heating prescribed in the model and the responding 300–hPa geopotential height responses were presented in Fig. 9 (Exps. 1 and 2 in Table 1). According to the spatial structure and magnitude of observational EP–type precipitation and associated diabatic heat (Fig. 3a), the heating sink (source) was placed onto the WP (EP) with a heating rate at the center of − 1.6 (1.3) K day^{-1} at the sigma level of 0.45 (Fig. 9a–c). Figure 10a shows the vertical profiles of the heat forcing over the WP and EP with a vertical extremum of − 1.6 and 1.3 K day^{-1} respectively. As a response to heat sink over the WP, an anomalous cyclonic and weak anticyclonic circulation appear over the subtropical WP at the upper level (Fig. 9a). On the contrary, the EP heating experiment is featured by a completely opposite pattern, with positive geopotential height anomaly over the tropics and negative nearby Japan (Fig. 9b). The joint effect of WP and EP heating anomalies is practically negligible (Fig. 9c). The responses to the WP and EP forcing are actually the
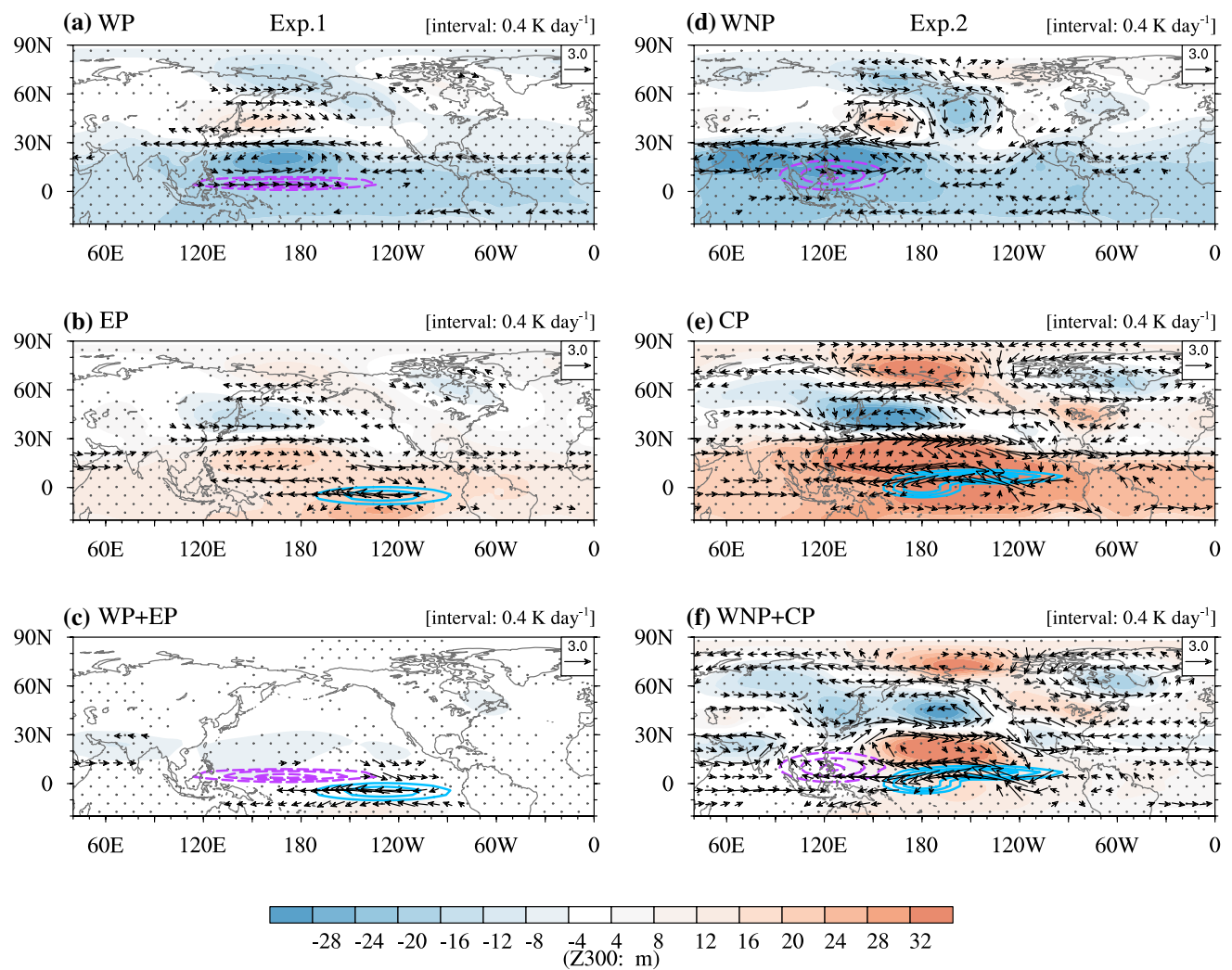
Fig. 9 Response of 300–hPa geopotential height (shading; unit: m) and horizontal winds anomalies (vector; unit: m s⁻¹) to the heat forcing over the **a** WP, **b** EP and **c** WP+EP with the basic state of 1980–1998 (Exp. 1 in Table 1) and **d** WNP, **e** CP and **f** WNP+CP with the basic state of 1999–2016 (Exp. 2 in Table 1). The contour shows the horizontal distribution of the heat forcing for each case at the sigma level of 0.45. The interval for heat forcing is 0.4 K day⁻¹. The stippling indicates significance of geopotential height at the 95% confidence level

Fig. 10 Vertical profile of the specific heating (K day⁻¹) at sigma levels in the cases of heat forcing **a** over the WP and EP during the pre–1998 period, **b** over the WNP and CP during the post–1999 period. Heat sink is dashed. The numbers in (**a**) and (**b**) represent the maximum and minimum heating rate at sigma level of 0.45
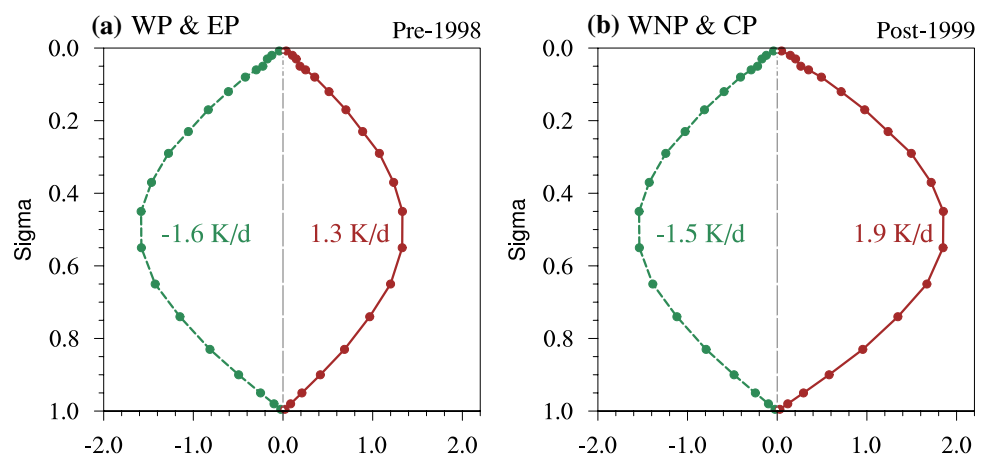
results adding the WP–only and EP–only numerical cases together due to the linearity of the LBM used in the present work. However, the experiment with both WP and EP forcing is still shown here to further investigate the joint contribution of precipitation anomaly over different regions to the variation of the teleconnection pattern clearly. Note that, in the case of sole EP heating, the anticyclonic center is located in the western North Pacific, far northwest to the heating center. Besides, the whole wave–like pattern excited by the EP heating seemly shifts westward and is slightly inconsistent with previous studies that focused on the ENSO induced circulation (Horel and Wallace 1981; Hoskins and Karoly 1981). This might be due to the boreal spring which is studied in our work. The tropical heat forcing for the EP type is placed more southeastward than the traditional precipitation distribution associated with the ENSO events. In addition, the subtle differences were also observed between the observations (Fig. 4b) and the model response of the Exp. 1. Previous studies have suggested that the transient eddy feedback may modify the extratropical responses to the tropical thermal forcing (Lin and Derome 1997, 2004). Hence, such differences between observation and simulation might be attributable to the lack of eddy forcing in the LBM. Besides, the idealized shape of heat forcing imposed into the model also may lead to some discrepancies. However, this problem is not fully understood and needs further analysis. Nonetheless, the model indeed produced a feeble atmospheric teleconnection, generally consistent with the observations. It gives a hint that the WP and EP precipitation, featured by a zonally elongated positive and negative anomalies, may have opposite effects on exciting the extratropical teleconnection patterns.

The CP–type precipitation pattern was idealized in LBM as an elliptic heat sink (source) over the WNP (CP) with a heating rate at the center of -1.5 (1.9) K day^{-1} at the sigma level of 0.45 (Fig. 9d–f) and their vertical profile were presented in Fig. 10b. Suppressed precipitation over the WNP could induce alternating cyclonic and anticyclonic circulations from the tropics to the Beaufort Sea (Fig. 9d). In contrast, enhanced precipitation anomalies with a comma–like shape over the CP is associated with a significant teleconnection pattern extending from tropic Pacific to the North Atlantic Ocean, which is featured by anomalous anticyclonic circulation along the north edge of precipitation center, cyclonic near Japan, anticyclonic over the Arctic Ocean and weak cyclonic circulation over the Baffin Island and Greenland (Fig. 9e). Thus, their conjunct impacts on the extra–tropical circulation (Fig. 9f) are mainly determined by the CP precipitation anomalies. Model simulation (Fig. 9f) shows high similarity to the observational result (Fig. 4d), though some subtle differences still can be found at mid–high latitudes. Overall, the model experiments in this

subsection add support to the conclusion that the CP–type precipitation mode could induce a significant teleconnection pattern from the subtropical CP to the North Atlantic Ocean.

5.2 Role of basic state in exciting teleconnection patterns

As mentioned in Sect 4.2, all of S1–S4, which delineate the interactive physical processes between heating–induced anomaly circulation and mean state, are conductive to the generation of Rossby wave during the post–1999 period. The role of mean state during the pre-1998 and post-1999 period in exciting different teleconnection patterns during the two periods will be addressed in this subsection.

First, the interdecadal differences of climatological divergence flow and absolute vorticity before and after 1998 were examined (Fig. 11). There is a significant positive center of absolute vorticity over the subtropical CP, indicating interdecadal intensification of absolute vorticity and change in the absolute vorticity gradient. They may affect the RWS variability through S1 and S3 terms. In addition, the divergence is enhanced over the WP and the southerly is also significantly reinforced over the subtropical CP during the post–1999 period (also could be seen in Figs. 7b and 8b). Thus, the RWS may be modulated by the changed mean divergence and divergence wind through S2 and S4 terms. Therefore, the observational evidence shows that the basic state indeed experiences a significant change during the two periods, especially over the subtropical CP. Question still remains whether such an interdecadal change in basic flow before and after 1998 is responsible for the teleconnection excitation and propagation. To figure it out, sensitive experiments to the basic state were performed (Exps. 3 and 4 shown in Table 1). Exp. 3 uses the EP–type heat forcing (WP and EP), together with the observed spring climatology
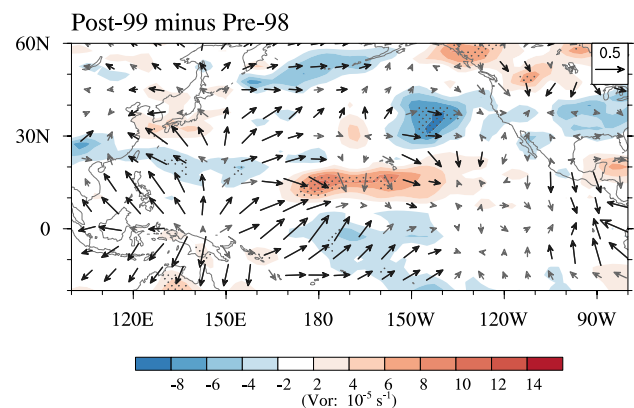
Fig. 11 The differences of mean absolute vorticity (shaded; unit: s^{-1}) and divergence wind (vector; unit: m s^{-1}) between the pre–1998 and post–1999 periods (post–1999 minus pre–1998). The stippling and thick vectors indicate differences at or above the 95% confidence level

for the post–1999 period, while Exp. 4 uses the CP–type heat forcing (WNP and CP) based on the climatology for the pre–1998 period. The comparison between Exps. 3 and 1 (Exps. 4 and 2) could help understanding the role played by changes of the basic state.

The model output of these two sensitive experiments are shown as Fig. 12. The result of Exp. 3 exhibits high similarity to that of Exp. 1 both the spatial patterns and the magnitude of atmospheric responses. Even though the mean state was replaced by the post–1999 climatology, the response to the EP–type precipitation mode is insignificant and shapeless. Similarly, the model result of Exp. 4 is analogous to that of Exp. 2, indicating that the change of spring basic state before and after 1998 is not a crucial factor that determines the generation and propagation of teleconnection patterns. The spatial distribution of the negative/positive precipitation anomalies seems to hold the key to the significant teleconnection appearance.

It is worthy to note that in traditional view the tropical precipitation pattern associated with the canonical El Niño was supposed to be related with a significant Pacific–North American (PNA)–like teleconnection in winter (Hoskins and Karoly 1981). However, the EP–type precipitation mode could not induce remarkable teleconnection in the present work. To figure it out, another sensitive experiment (EP–type heat forcing with the winter–mean basic state) was carried out using the LBM. It was found that the EP–type precipitation pattern identified in our work could excite a PNA–like teleconnection with the basic flow in winter (figure not shown). Considering the ineffectively generation of a poleward wave train in spring (Fig. 9c), hence, the atmospheric responses to thermal forcing in spring is quite different from that in winter. It was demonstrated that the basic state change between 1980 and 1998 and 1999–2016 in spring plays a trivial role in the excitation of teleconnection pattern, however, the differences of the basic flow between
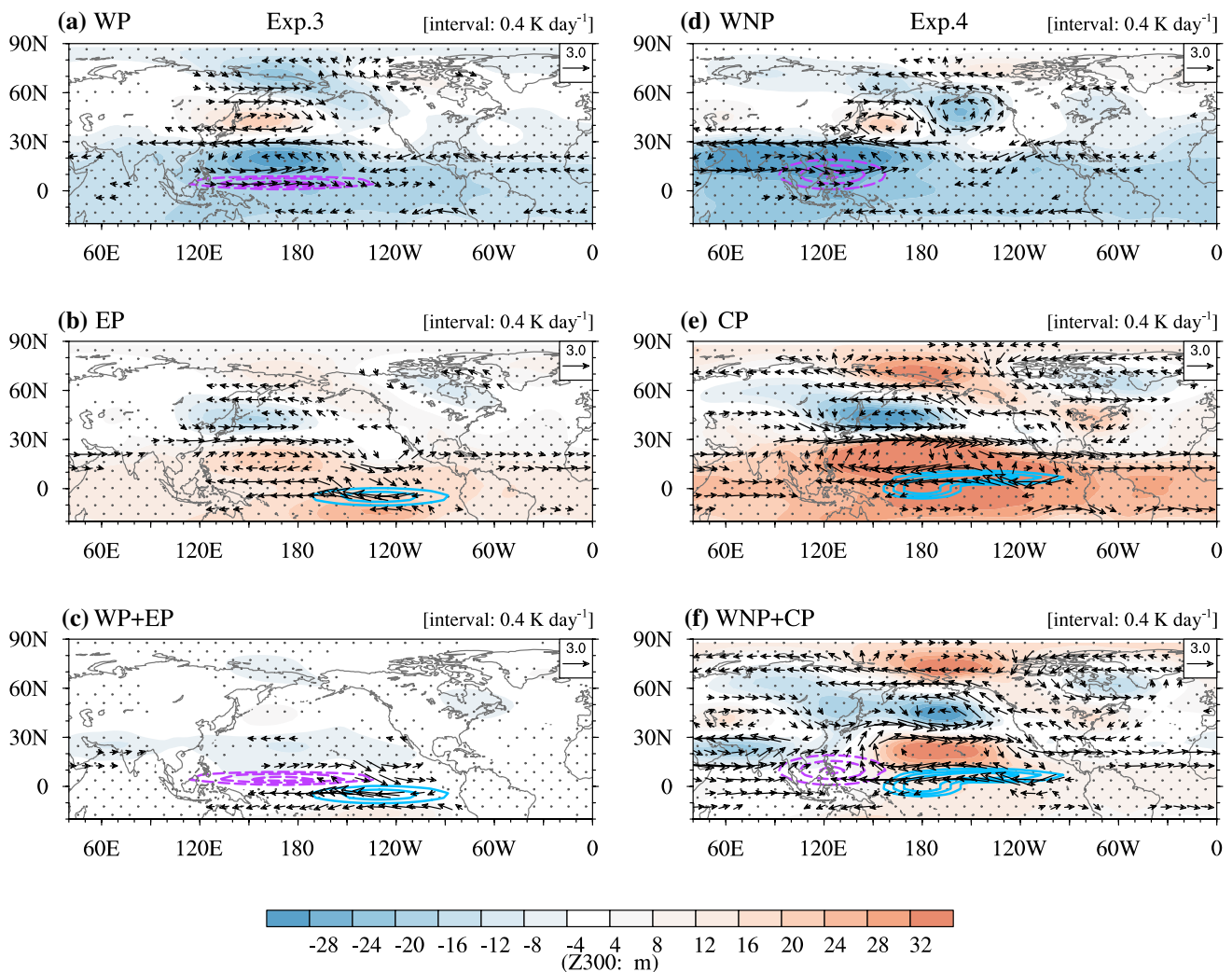

Fig. 12 Same as Fig. 9, but for the Exps. 3 and 4

the winter and spring could result in extremely distinguishable teleconnection patterns.

6 Summary and discussion

Our previous study (GWW2016) has shown that the leading mode of precipitation anomaly in spring shifted from an EP–type to a CP–type pattern around the late 1990s. Following this work, we attempted to investigate the robustness of such an interdecadal change in the main precipitation mode after the 2015/16 super El Niño occurred and to explore the impact of two distinct precipitation anomaly patterns on the extratropical teleconnection in current study. The case study of 2016 spring found that the tropical Pacific precipitation anomaly pattern is featured by a zonal dipole pattern with positive precipitation anomalies over the CP and negative over the WNP, highly similar to the CP–type precipitation mode. The EOF analyses during the 1980–2016 period added support to the significance of the interdecadal change in main precipitation mode in spring after 1998. Consequently, it has been demonstrated that the spring precipitation interannual variability over the tropical Pacific displays a remarkable interdecadal change in its leading mode after 1998.

Further analyses revealed that the CP–type precipitation mode is closely related to a significant teleconnection pattern extending from the tropics to North Atlantic Ocean, while the teleconnection associated with the EP–type precipitation mode is unclear. It suggested that extratropical circulation may experience an interdecadal change of the interannual variation due to the shift of precipitation mode in spring over the Pacific Ocean. To detect the mechanisms of such teleconnection pattern after 1998, both the RWS and horizontal component of Plumb flux were examined. It turned out that only for CP–type precipitation mode during the post–1999 period, significant RWS anomalies over the subtropical CP and clear Rossby wave propagation from the tropics to Arctic Pole were detected. It was suggestive of effective generation and propagation of Rossby wave for the CP–type precipitation mode while weak forcing of Rossby wave for the EP–type. From the perspective of vorticity generation balance, we found that for the pre–1998 EP–type precipitation mode, the vortex stretching term was offset by the absolute vorticity advection term to a large extent over the subtropical Pacific due to the feeble divergence flow and shapeless vorticity anomaly induced by the anomalous precipitation. For the post–1999 CP–type precipitation mode, the specific distribution could result in strong divergent southerly and well–organized negative vorticity anomaly, leading to the effective contribution of the vortex stretching and absolute vorticity advection terms to the total RWS. It was indicative of significant generation of vorticity source

and propagation of Rossby wave for the CP–type precipitation pattern.

Results from several model experiments in LBM further confirm the distinct teleconnection behavior induced by different precipitation patterns. For EP–type precipitation mode, the influence of negative precipitation anomalies over the WP on the teleconnection is opposite to that of positive precipitation anomalies over the EP. Hence, the teleconnection pattern jointly contributed by them is weak and insignificant. In contrast, the model response to the CP–type precipitation mode greatly resembles the observational teleconnection pattern, with anticyclonic anomalies over the subtropical CP, cyclonic circulation over the central North Pacific, anticyclonic over the Arctic Sea and cyclonic circulation over the North Atlantic. In particular, the contribution of the comma–shaped precipitation anomalies over the CP is dominant. As a result, the model results by LBM proved that the EP–type precipitation mode cannot induce significant teleconnection pattern, while the CP–type precipitation mode could excite an apparent poleward–propagating teleconnection pattern due to its specific location and spatial distribution of negative/positive precipitation anomalies. Experiments decided to inspect the sensibility to the basic state suggested that the change in the spring basic flow before and after 1998 plays a minor role in inducing extratropical teleconnection compared with the tropical precipitation forcing.

To summarize, the interdecadal change in the precipitation anomaly mode in spring over the tropical Pacific could exert tremendous impacts on the extratropical teleconnection variability. However, there are still subtle differences between the model simulations and observational results. For instance, the observational anomalous cyclonic circulation over the central North Pacific is stronger and the anticyclonic circulation over the western Canada shifts more southeastward than the model's responses (Figs. 4d and 9f). These differences at mid–high latitudes between model results and observations might be attributed to the lack of transient eddy feedback in LBM. Hence, the role of transient eddy activity in heating–inducing teleconnection patterns needs further examination in the future work.

References

Adler RF, Huffman GJ, Chang A et al (2003) The Version-2 global precipitation climatology project (GPCP) monthly precipitation

analysis (1979–Present). J Hydrometeorol 4:1147–1167. https://doi.org/10.1175/1525-7541(2003)004<1147:TVGPCP>2.0.CO;2

Ashok K, Behera SK, Rao SA et al (2007) El Niño Modoki and its possible teleconnection. J Geophys Res Ocean 112:1–27. https://doi.org/10.1029/2006JC003798

Black RX, Dole RM (1993) The dynamics of large-scale cyclogenesis over the North Pacific Ocean. J Atmos Sci 50:421–442. https://doi.org/10.1175/1520-0469(1993)050<0421:TDOLSC>2.0.CO;2

Cai W, Cowan T (2009) La Niña Modoki impacts Australia autumn rainfall variability. Geophys Res Lett 36:9–12. https://doi.org/10.1029/2009GL037885

Chen Z, Du Y, Wen Z et al (2017) Indo-Pacific climate during the decaying phase of the 2015/16 El Niño: role of southeast tropical Indian Ocean warming. Clim Dyn. https://doi.org/10.1007/s00382-017-3899-z

Chu C, Yang XQ, Ren X, Zhou T (2013) Response of Northern Hemisphere storm tracks to Indian-western Pacific Ocean warming in atmospheric general circulation models. Clim Dyn 40:1057–1070. https://doi.org/10.1007/s00382-013-1687-y

Chu C, Yang X-Q, Sun X et al (2017) Effect of the tropical Pacific and Indian Ocean warming since the late 1970s on wintertime Northern Hemispheric atmospheric circulation and East Asian climate interdecadal changes. Clim Dyn 22:1–18

Chung P-H, Li T (2013) Interdecadal relationship between the mean state and El Niño types. J Clim 26:361–379. https://doi.org/10.1175/JCLI-D-12-00106.1

Dee DP, Uppala SM, Simmons AJ et al (2011) The ERA-Interim reanalysis: configuration and performance of the data assimilation system. Q J R Meteorol Soc 137:553–597. https://doi.org/10.1002/qj.828

Feng J, Li J (2011) Influence of El Niño Modoki on spring rainfall over south China. J Geophys Res Atmos 116:1–10. https://doi.org/10.1029/2010JD015160

Feng J, Chen W, Tam CY, Zhou W (2011) Different impacts of El Niño and El Niño Modoki on China rainfall in the decaying phases. Int J Climatol 31:2091–2101. https://doi.org/10.1002/joc.2217

Guo Y, Wen Z, Wu R et al (2015) Impact of tropical Pacific precipitation anomaly on the East Asian upper-tropospheric westerly jet during the boreal winter. J Clim 28:6457–6474. https://doi.org/10.1175/JCLI-D-14-00674.1

Guo Y, Wen Z, Wu R (2016) Interdecadal change in the tropical pacific precipitation anomaly pattern around the late 1990s during boreal spring. J Clim 29:5979–5997. https://doi.org/10.1175/JCLI-D-15-0462.1

Guo Y, Ting M, Wen Z, Lee DE (2017) Distinct patterns of tropical Pacific SST anomaly and their impacts on North American climate. J Clim 30:5221–5241. https://doi.org/10.1175/JCLI-D-16-0488.1

Horel JD, Wallace JM (1981) Planetary-scale phenomena associated with the Southern Oscillation. Mon Weather Rev 109:813–829

Hoskins BJ, Ambrizzi T (1993) Rossby wave propagation on a realistic longitudinally varying flow. J Atmos Sci 50:1661–1671

Hoskins BJ, Karoly DJ (1981) The steady linear response of a spherical atmosphere to thermal and orographic forcing. J Atmos Sci 38:1179–1196

Jacox MG, Hazen EL, Zaba KD et al (2016) Impacts of the 2015–2016 El Niño on the California current system: early assessment and comparison to past events. Geophys Res Lett 43:7072–7080. https://doi.org/10.1002/2016GL069716

Jia X, Wang S, Lin H, Bao Q (2015) A connection between the tropical Pacific Ocean and the winter climate in the Asian–Pacific region. J Geophys Res Atmos 120:430–448. https://doi.org/10.1002/2014JD022324

Jo H-S, Yeh S-W, Lee S-K (2015) Changes in the relationship in the SST variability between the tropical Pacific and the North

Pacific across the 1998/99 regime shift. Geophys Res Lett 42:7171–7178. https://doi.org/10.1002/2015GL065049

Johnson NC, Kosaka Y (2016) The impact of eastern equatorial Pacific convection on the diversity of boreal winter El Niño teleconnection patterns. Clim Dyn 47:3737–3765. https://doi.org/10.1007/s00382-016-3039-1

Kosaka Y, Nakamura H (2006) Structure and dynamics of the summertime Pacific–Japan teleconnection pattern. Q J R Meteorol Soc 132:2009–2030. https://doi.org/10.1256/qj.05.204

Lim YK, Kovach RM, Pawson S, Vernieres G (2017) The 2015/16 El Niño event in context of the MERRA-2 reanalysis: a comparison of the tropical pacific with 1982/83 and 1997/98. J Clim 30:4819–4842. https://doi.org/10.1175/JCLI-D-16-0800.1

Lin H, Derome J (1997) On the modification of the high- and low-frequency eddies associated with the PNA anomaly: an observational study. Tellus Ser A Dyn Meteorol Oceanogr 49:87–99. https://doi.org/10.3402/tellusa.v49i1.12213

Lin H, Derome J (2004) Nonlinearity of the extratropical response to tropical forcing. J Clim 17:2597–2608. https://doi.org/10.1175/1520-0442(2004)017<2597:NOTERT>2.0.CO;2

Lu R, Kim B-J (2004) The climatological Rossby wave source over the STCZs in the summer northern hemisphere. J Meteorol Soc Japan 82:657–669. https://doi.org/10.2151/jmsj.2004.657

Lu R, Lin Z (2009) Role of subtropical precipitation anomalies in maintaining the summertime meridional teleconnection over the western North Pacific and East Asia. J Clim 22:2058–2072. https://doi.org/10.1175/2008JCLI2444.1

McBride JL, Haylock MR, Nicholls N (2003) Relationships between the maritime continent heat source and the El Niño-Southern oscillation phenomenon. J Clim 16:2905–2914. https://doi.org/10.1175/1520-0442(2003)016<2905:RBTMCH>2.0.CO;2

Paek H, Yu JY, Qian C (2017) Why were the 2015/2016 and 1997/1998 extreme El Niños different? Geophys Res Lett 44:1848–1856. https://doi.org/10.1002/2016GL071515

Park J-H, An S-I (2014) The impact of tropical western Pacific convection on the North Pacific atmospheric circulation during the boreal winter. Clim Dyn 43:2227–2238. https://doi.org/10.1007/s00382-013-2047-7

Peng S, Whitaker JS (1999) Mechanisms determining the atmospheric response to midlatitude SST anomalies. J Clim 12:1393–1408. https://doi.org/10.1175/1520-0442(1999)012<1393:MDTART>2.0.CO;2

Plumb RA (1985) On the three-dimensional propagation of stationary waves. J Atmos Sci 42:217–229

Rayner NA, Parker DE, Horton EB et al (2003) Global analyses of sea surface temperature, sea ice, and night marine air temperature since the late nineteenth century. J Geophys Res 108:4407. https://doi.org/10.1029/2002JD002670

Sardeshmukh PD, Hoskins BJ (1988) The generation of global rotational flow by steady idealized tropical divergence. J Atmos Sci 45:1228–1251

Shimizu MH, de Cavalcanti IFA (2011) Variability patterns of Rossby wave source. Clim Dyn 37:441–454. https://doi.org/10.1007/s00382-010-0841-z

Taschetto AS, England MH (2009) El Niño Modoki Impacts on Australian Rainfall. J Clim 22:3167–3174. https://doi.org/10.1175/2008JCLI2589.1

Wallace JM, Gutzler DS (1981) Teleconnections in the geopotential height field during the northern hemisphere winter. Mon Weather Rev 109:784–812

Wang J, Wen Z, Wu R et al (2016) The mechanism of growth of the low-frequency East Asia–Pacific teleconnection and the triggering role of tropical intraseasonal oscillation. Clim Dyn 46:3965–3977. https://doi.org/10.1007/s00382-015-2815-7

Watanabe M, Kimoto M (2000) Atmosphere–ocean thermal coupling in the North Atlantic: a positive feedback. Q J R Meteorol Soc 126:3343–3369. https://doi.org/10.1002/qj.49712657017

Webster PJ, Chang H-R (1998) Atmospheric wave propagation in heterogeneous flow: basic flow controls on tropical—extratropical interaction and equatorial wave modification. Dyn Atmos Ocean 27:91–134. https://doi.org/10.1016/S0377-0265(97)00003-1

Weng H, Behera SK, Yamagata T (2009) Anomalous winter climate conditions in the Pacific rim during recent El Niño Modoki and El Niño events. Clim Dyn 32:663–674. https://doi.org/10.1007/s00382-008-0394-6

Wu B, Zhou T, Li T et al (2012) Two distinct modes of tropical indian ocean precipitation in boreal winter and their impacts on equatorial Western Pacific. J Clim 25:921–938. https://doi.org/10.1175/JCLI-D-11-00065.1

Yoo C, Lee S, Feldstein SB (2012) Mechanisms of arctic surface air temperature change in response to the Madden–Julian oscillation. J Clim 25:5777–5790. https://doi.org/10.1175/JCLI-D-11-00566.1

Yu B, Zwiers FW (2007) The impact of combined ENSO and PDO on the PNA climate: A 1000-year climate modeling study. Clim Dyn 29:837–851. https://doi.org/10.1007/s00382-007-0267-4

Zheng J, Liu Q, Wang C, Zheng XT (2013) Impact of heating anomalies associated with rainfall variations over the Indo–Western Pacific on Asian atmospheric circulation in winter. Clim Dyn 40:2023–2033. https://doi.org/10.1007/s00382-012-1478-x